Proceedings of IMECE'03
2003 ASME International Mechanical Engineering Congress
Washington, D.C., November 15–21, 2003

IMECE2003-41450

SIMULATION AND DESIGN AN E. COLI-BASED ROTARY MICROPUMP FOR USE IN MICROFLUIDIC SYSTEMS: INTEGRATION OF MICRO-NANO-BIO

Mohamed G. Al-Fandi, Microelectronics-Photonics program, University of Arkansas, Fayetteville, 72701

Ajay P. Malshe*, SERC-MRL, Mechanical Engineering, Department, University of Arkansas, Fayetteville, 72701; ** Contacting author- apm2@engr.uark.edu, Phone: 479-575-6561*

Shankar Sundaram, CFD Research Corporation, Huntsville, AL 35805

Jerry Jenkins, CFD Research Corporation, Huntsville, AL 35805

Steve Tung, Mechanical Engineering Department, University of Arkansas, Fayetteville, 72701

Jin-Woo Kim, Biological and Agricultural Engineering Department, University of Arkansas, Fayetteville, 72701

ABSTRACT

This paper presents the results of the computational fluid dynamic (CFD) modeling of viscous fluid flow in a novel cell motor actuated micropump. A cell motor is a bacterial flagellar cell tethered to a surface by a single flagellum, this flagellum acts as a pivot around which the cell body rotates. As a test case for investigation, the micropump consisted of two *Escherichia coli* cell motors tethered to the bottom of a microchannel with fixed dimensions. The CFD modeling of the micropump was performed using CFD-ACE$^+$ simulation software (CFD Research Corporation). The biological cell motor was modeled as an ellipse with constant rotational speed of 10 Hz clockwise. The results of this model demonstrated the effect of the biological cell motor placement within the microchannel, as well as the rotational phase between the two biological cell motors, on the volumetric flowrate. Pumping action was observed as the cell motor location was moved adjacent to the sidewall of the microchannel. The rates of fluid pumping were of the order of 11 pL/hr when the cell motors were rotating in phase and their placement was close to the sidewall of the microchannel.

NOMENCLATURE

Biological cell motor, computational fluid dynamics, *E. coli*, finite-volume, microchannel, microfluidic, micropump.

INTRODUCTION

Integration of micro-nano-bio is a critical and challenging philosophy for the next generation of engineered systems. In particular, the adaptation of unique features such as self powered, thinking, self-healing, etc. in synthetically manufactured systems is essential for advanced applications such as bio-medical, on-demand sensing and actuation, on-demand information-to-knowledge transduction, etc. The cell-motor based micropump, which is the focus of this paper, is an example of such next generation systems. The cell motor micropump applies nano sized flagellar motors along with the micro cells to actuate the fluid flow in a typical microchannel environment. The following engineering challenges make this system interesting: realization of unidirectional cell-motor actuation, application specific placement of cells in the microchannels, designing of flagella-substrate interfaces, understanding the effect of cell motor rotation in and out of phase on fluid flow, lifetime of these systems, etc. Particularly, the following discussion is a focused attempt to understand the effect of cell motor parameters on fluid flow dynamics using a methodical simulation approach.

During the past fifteen years, different types of MEMS-based micropumps have been reported. These include non-mechanical and mechanical actuated micropumps. The electro-hydrodynamic [1], the electro-osmotic [2], the electro-kinetic [3], and the thermal [4] methods were utilized to actuate the non-mechanical micropumps. The electrostatic [5], the piezoelectric [6], and the pneumatic [7] methods were utilized to actuate the positive displacement mechanical micropumps. Unlike state-of-the-art MEMS actuation mechanisms, the biological cell motors work using naturally synthesized flagellar motors located at the cell wall [8]. These motors

receive nutrients from the fluid and start rotating under specific bio-chemical conditions. These self-powered and environment-specific switching characteristics make these motors and their integration at the cell-microchannel boundary unique for a self actuated viscous micropump. This viscous micropump uses rotary motion of the cell to generate a surface force, thereby creating fluid flow, and thus it is well suited for extremely low Reynolds number microfluidics. The viscous effects in fluid devices have been theoretically discussed by numerous research efforts [9,10,11]. And various MEMS-based viscous micropump versions have been numerically analyzed [12]. Yet, designing and fabrication of a MEMS-based viscous micropump pose major technical challenges. The design and fabrication of the actuation element, which is capable of rotating 360-degrees, is always difficult due to large friction force and the need for complex actuation mechanisms. Alternatively, biological rotary motors may be a promising actuation mechanism, as they serve as the rotating elements in the viscous micropump.

In analysis of MEMS-based viscous micropumps, three-dimensional Navier-Stokes equations were solved by using finite-element algorithms [12]. While the finite-element approach is suited for low Reynolds number situations, the finite-volume method is a better choice due to the rigorous conversation of physical quantities.

In this paper, the use of the finite-volume method is focused on analyzing the fluid flow generated by a cell motor in a micropump. The effect of cell motor selective placement inside a microchannel and the rotation phase of the cell motors on the volumetric flowrate of the micropump are demonstrated in this paper.

GEOMETRY AND APPLIED BOUNDARY CONDITIONS

Figure 1 illustrates the representative micropump under investigation. Non-pathogenic *E. coli* bacteria actuate the viscous biological micropump. Each biological cell motor was modeled as an ellipse like shape with a length of 3 µm, width of 0.5 µm, and depth of 0.5 µm, which is the typical geometry of *E. coli* cell. The investigation was carried out for two test cases; a single cell motor and dual cell motors. In the single cell motor case, the biological cell motor was placed at the center of a microchannel and then repositioned, in steps, toward the sidewall of the microchannel. The cell motor was located 0.5 µm above the bottom of the microchannel, which is typical body location of a tethered an *E. coli* cell. On the other hand, the dual cell motors case was utilized to investigate the effect of the rotational phase of cell motors on the volumetric flowrate. The center of the cell motors was placed 2.1 µm from the sidewall of the microchannel. The cell motors were located 4.6 µm apart (center-to-center). The distance between the cell motors was optimized as the fluid velocity profiles between the adjacent cell motors started to interact.

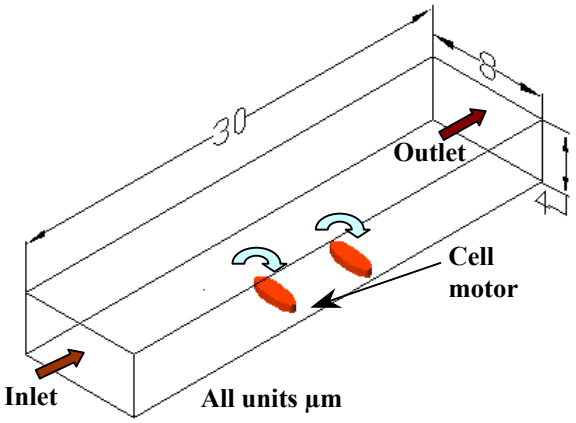

Figure 1. Microchannel geometry with the cell motors.

At the sidewalls of the microchannel and the outer membrane of the cell motors, the no slip boundary condition was used. However, for the conditions at the inlet and outlet, fluid was allowed to freely pass into and out of the control volume, with the pressure being set to an ambient value of 100 kPa. Moreover, the inlet and outlet were located far enough to minimize the effect of the pressure and the velocity constrain on these boundary conditions. In both cases, the biological cell motors were rotating at constant speed of 10 Hz. This rotational speed is typical when *E. coli* cells are tethered to a glass surface at room temperature and pH 7.0 [8,13].

GRID GENERATION AND FLUID PROPERIES

The geometry of the micropump was built using a structured grid method, which is based on the transfinite interpolation (TFI) methodology (Figure 2). The grid density around the biological cell motors was maximized to accurately capture the change of the fluid properties as the rotation of the cell motors takes place. Moreover, the sensitivity of the grid density was tested by changing the number of grid cells and monitoring the change in the velocity profile and the volumetric flowrate. The optimum value of the cell density is achieved when the change of the number of gird cells has minimal effect on the monitored values. Additionally, a sliding interface between stationary grid and moving grid was utilized to allow the rotation without grid deformation.

As the geometry was built using a blocks method, all fluid blocks were assigned to have constant fluid properties. In view of the fact that more than 90% of the *E. coli* motility medium consists of water, the fluid dynamics simulation utilized the properties of water at room temperature.

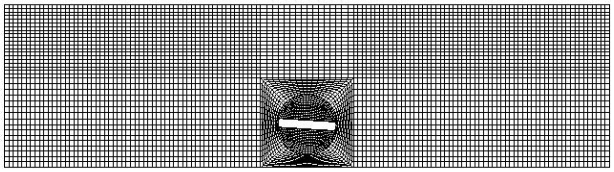

A) Single cell motor grid

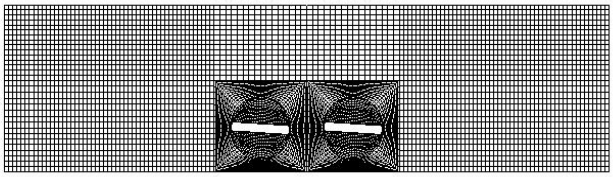

B) Dual cell motors grid

Figure 2. Structured grid around the cell motors.

FLOW SOLVER AND NUMERICAL METHODS

The governing equations are the time dependent Navier-Stokes equations which express the conservation laws of mass, momentum, total enthalpy, and other definable scalar quantities. They are equally applicable to incompressible and compressible flows. Numerical solution of this equation set requires discretization of the computational domain into a large number of generalized control volumes. To allow full freedom in the control volume shapes the governing equations are expressed into the integral flux form shown below:

$$\frac{\partial}{\partial t}\int_v \rho dv + \oint_\sigma \rho\left(\vec{V} - \vec{V}_g\right)\cdot \vec{n} d\sigma = 0 \tag{1}$$

$$\begin{aligned}\frac{\partial}{\partial t}\int_v \rho u_i dv + \oint_\sigma \rho\left(\vec{V} - \vec{V}_g\right)\cdot \vec{n} u_i d\sigma = \\ -\oint_\sigma p n_i d\sigma + \oint_\sigma \tau_{ij} n_j d\sigma + \int_v f_i dv\end{aligned} \tag{2}$$

$$\begin{aligned}\frac{\partial}{\partial t}\int_v \rho h_t dv + \oint_\sigma \rho\left(\vec{V} - \vec{V}_g\right)\cdot \vec{n} h_t d\sigma = \\ \oint_\sigma q_j n_j d\sigma + \int_v \frac{\partial p}{\partial t} dv + \oint_\sigma \tau_{ij} u_j n_i d\sigma + \int_v f_i u_i dv\end{aligned} \tag{3}$$

$$\tau_{ij} = \left(\mu + \mu_t\right)\left(\frac{\partial u_i}{\partial x_j} + \frac{\partial u_j}{\partial x_i}\right) - \frac{2}{3}\left(\mu + \mu_t\right)\left(\frac{\partial u_k}{\partial x_k}\right)\delta_{ij} \tag{4}$$

$$q_j = k\frac{\partial T}{\partial x_j} \tag{5}$$

Where u_i is the i^{th} Cartesian component of the velocity, V_g is the grid velocity due to grid motion, p is the static pressure, h_t is the total enthalpy, τ_{ij} is the stress tensor for both laminar and turbulent flows, and f_i is the i^{th} Cartesian component of the body force.

The baseline solver in the CFD-ACE+ software package is a 3D pressure-based Navier-Stokes solver developed by Jiang and Przekwas [14]. The software is capable of solving fluid flow on a mixed unstructured, quadrangle, tetrahedral, hexahedra, prismatic and pyramid. The code accuracy and robustness have been demonstrated on a wide variety of 2D and 3D geometries and conditions [15]. The flow solver can also handle sliding interfaces. A sliding interface is the interface used to connect a moving grid with a stationary grid. The implementation used here is a fully implicit and fully conservative general implementation [16].

Navier-Stokes equations were numerically solved for laminar incompressible flow at room temperature to investigate the fluid dynamics inside the *E. coli* cell motor-based micropump. Furthermore, the convergence of the numerical solution of Navier-Stokes equations was declared at a five order of magnitude reduction in the residual of the velocity.

CASE I: EFFECT OF SINGLE CELL MOTOR LOCATION IN A MICROCHANNEL

The cell motor-based micropump takes advantage of the shear driven flow to transport fluids inside microgeometries. In the shear driven flow, the rotating biological cell motors create a fluid velocity profile. The pumping action occurs when one of the fluid velocity components around the cell motors is eliminated. As can be seen in Figure 3, when the biological cell motor was placed on the center of a microchannel, the net volumetric flowrate was tending to zero. However, as the cell motor was repositioned farther from the center and nearer to the sidewall of the microchannel, the pumping action took place. As the cell motor was brought closer to the sidewall of the microchannel the net volumetric flowrate increased. However, the increasing rate of the volumetric flowrate became marginally less when the center of the cell motor was at 2.1 μm from the sidewall of the microchannel. This observation is

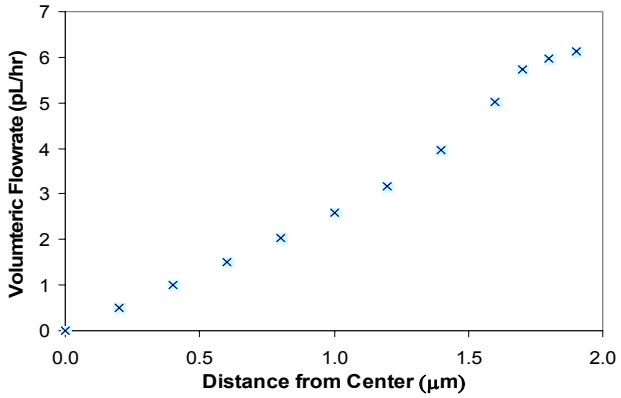

Figure 3. Effect of single cell motor location on the volumetric flowrate.

likely to be due to the decrease of the gap between the body of the cell motor and the sidewall of the microchannel, which results in accelerating the back flow. Consequently, the increasing rate of the volumetric flowrate was slowed down.

In designing the cell motor-based micropump, the curve in Figure 3 was utilized to determine the optimum location of the cell motor. The location of the cell motor was selected as such when the increasing rate of the net volumetric flowrate started to slow down (i.e. at 2.1 μm from the sidewall of the microchannel). Moreover, from the fabrication perspective, the placement of cell tethering pads at this location is a realistic prospect.

CASE II: EFFECT OF ROTATIONAL PHASE OF THE CELL MOTORS

The envisioned cell motor-based micropump will utilize more than one cell motor, for example patterned in desired array configuration, to overcome the viscous loss as the fluid flow propagates downstream of a microchannel. Yet, controlling the phase between adjacent cell motors is currently a difficult task to achieve, due to the inherent uncertainties and lack of precision control on biological micro and nano "components". Thus, this section is dedicated to discussing the effect of the rotational phase between adjacent cell motors on the pumping action.

Figure 4 shows a schematic of the rotational phase investigation. The cell motor on the right side in Figure 4 was situated at zero angle while the angle Θ of the cell motor on the left side was varied. With a sampling frequency of Θ=15°, the volumetric flowrate at the outlet of the microchannel was calculated.

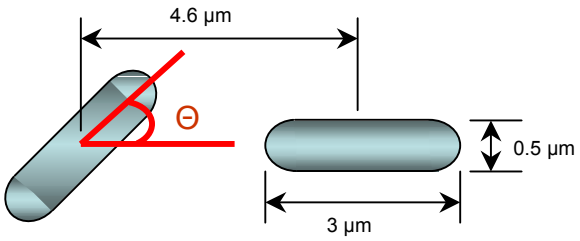

Figure 4. Rotational phase angle between cell motors.

The results of this investigation showed that a volumetric flowrate of 11 pL/hr can be obtained when the cell motors are in phase. However, as can be seen in Figure 5, a 5% decrease in the net volumetric flowrate was observed when the cell motors are 90° out of phase. This observation was because the flow was assumed to be continuum and incompressible. In the continuum assumption, the properties of the fluid are not allowed to become infinite or jump discontinuously at a single point. Also, the density remains constant in the flow as the incompressibility suggests. Moreover, the fluid is being

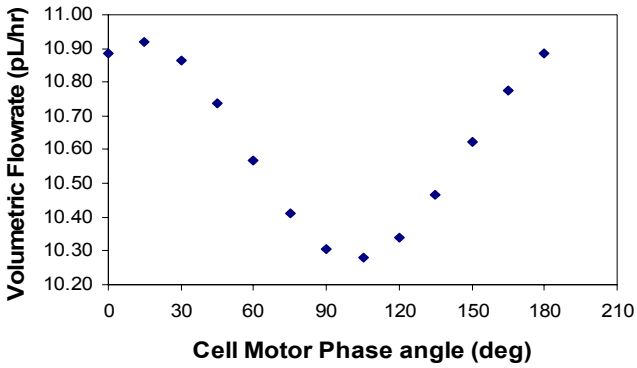

Figure 5. Effect of cell motors rotational phase on the volumetric flowrate.

transported at an extremely low Reynolds number, and thus, the flow will have enough time to adjust itself and sense the adjacent cell motor.

To understand how the fluid flow behaves as it propagates throughout the microchannel, the fluid velocity profiles around the cell motors were obtained. Figure 6 shows the contour representations of fluid velocity across the microchannel when the cell motors are in phase. In Figure 6a the velocity contours have sequential forward and backward velocity while the contours have no extension toward the inlet or the outlet of the microchannel. A forward velocity is a velocity toward the outlet of the microchannel, while the backward velocity is toward the

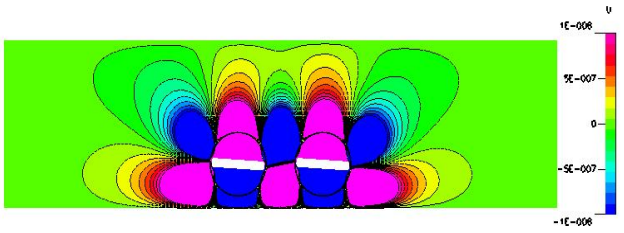

a) 0° and 180° rotation angle

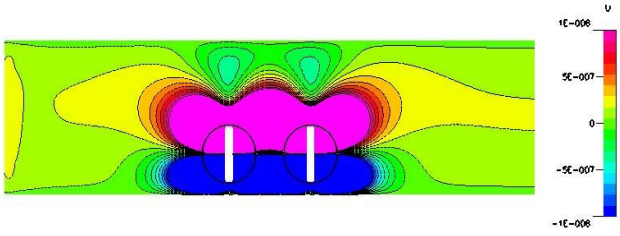

b) 90° and 270° degree rotation angle

Figure 6. Velocity distributions when the cell motors are in phase.

inlet of the microchannel. Figure 6a suggests that the net volumetric flowrate at this rotation angle is almost zero (i.e. at zero and 180^o angles). On the other hand, as shown in Figure 6b, the velocity contours have a forward velocity component at one side of the cell motors and a backward velocity component at the other side. In this study, the backward velocity component was targeted for elimination. Furthermore, the velocity contours have forward extensions toward the inlet and the outlet of the microchannel, which proposes that a net positive volumetric flowrate can be obtained at this rotation angle (i.e. at 90^o and 270^o angles). Figures 6a and 6b suggest that the fluid flow is pulsating through out the rotation of the cell motors when they are rotating in phase.

Figure 7 shows the fluid velocity contours when the cell motors are rotating at 90^o out of phase. In the Figures (Figure 7a and 7b), the fluid velocity profiles showed sequential forward and backward velocity components. Furthermore, a forward velocity component was extended toward the inlet and the outlet of the microchannel. This suggests that a continuous fluid flow might be obtained when the cell motors are rotating 90^o out of phase.

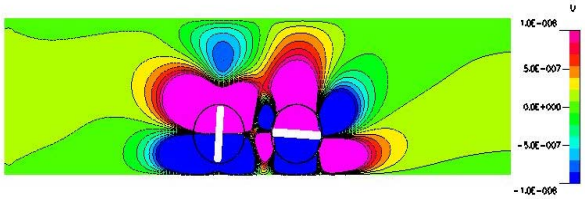

a) 0^o and 180^o rotation angle

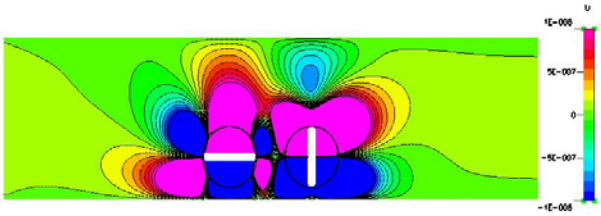

b) 90^o and 270^o rotation angle

Figure 7. Velocity distributions when the cell motors are 90^o out of phase.

CONCLUSIONS

In this study, the authors showed the simulation approach for studying cell motor pumping. Pumping action occurs when the cell motors are brought closer to the sidewall of a microchannel. The rotational phase of the adjacent cell motors affects the nature of the volumetric flowrate, as well as the total net volumetric flowrate. When the cell motors are rotating in phase, the net volumetric flowrate can be maximized with pulsating flow. However, a continuous net volumetric flowrate might be obtained when the cell motors are rotating at 90^o out of phase. Currently, unlike a MEMS device, precise control on the rotational phase of the cell motors is a challenging task to achieve.

The *E.coli*-based rotary micropump delivers extremely low volumetric flowrate, which makes it well suited as a localized micropump for cleaning and supplementary pumping purposes in micro-nanofluidics systems. Further, their self-power and sensing ability make them suitable candidates for biomedical applications.

The authors are currently developing a chemo-mechanical model to investigate the effect of the H^+ flux to the cell motors on the rotational speed of the cell motors. The model will be accompanied with an experimental study.

ACKNOWLEDGMENTS

Authors thankfully acknowledge the National Science Foundation, NSF-IGERT (Award # DGE-9972820), NSF-EPSCOR (Award #9977830) and the Division of Electrical and Communications Systems (Award # 0201004) for the support of this work.

REFERENCES

[1] Bart, S. F., Tavrow L. S., Mehregany, M., and Lang, J. H., 1990, "Microfabrication Electrohydrodynamic Pump," Sensors and Actuators A, A21, pp. 193-197.

[2] Harrison, D. J., Fan, K. F., and Seiler, K., 1994, "Integrated Eletcrophoresis Systems for Biochemical Analysis," Technical Digest of the 1994 Solid State Sensor and Actuator Workshop, pp. 21-24.

[3] Chen, C.H., Zeng, S., Mikkelsen, J.C., and Santiago, J.G., 2000, "Microfabricated electrokinetic micropump," Abstracts of Papers of The American Chemical Society V. 219 (Pt.1) pp. 431-Coll, Mar 26-30.

[4] Hung, T., and Lin, L., 2002, "A Thermal Bubble Actuated Micro Nozzle-Diffuser pump," Journal of Microelectromechanical Systems, Vol. 11, No. 6, pp. 665-671.

[5] Jiang, T., Ng, T., and Lam, K., 2000, "Dynamic Analysis of an Electrostatic Micropump," Technical Proceedings of the 2000 International Conference on Modeling and simulation of Microsystems, San Diego, California, March 27-29.

[6] Ullmann, A., 1998, "The piezoelectric valve-less pump performance enhancement analysis," Sensors and Actuators A, A 69:97–105.

[7] F.C.M. van de Pol, H.T.G. van Lintel, M/Elwenspoek, and J.H.J. Fluiman, 1990, "A Thermopeneumatic Micropump Based on Micro-engineering Techniques," Sensors and Actuators A, pp. 21-23.

[8] Howard C. Berg, 2003, “The Rotary Motor of Bacterial Flagella,” Annu. Rev. Biochem., **72**, pp. 19-54.

[9] Hellou, M., and Coutanceau, M., 1992, “Cellular Stokes Flow Induced by Rotation of a Cylinder in a Closed Channel,” Journal of Fluid Mechanics, Vol. 236, pp. 557-577.

[10] Ingham, D.B., and Tang, T., 1990, “A Numerical Investigation into the Steady Flow Past a Rotating Cylinder at Low and Intermediate Reynolds Numbers,” Journal of Computational Physics, Vol. 87, pp. 91-107.

[11] Kimura, T., Tsutahara, M., and Wang, Z., 1992, “Wake of a Rotating Circular Cylinder,” AIAA Journal, Vol. 30, pp. 555-556.

[12] Decourtye, D., Sen, M., and Gad-el-Hak, M., 1998, “Analysis of Viscous Micropumps and Microturbines,” International Journal of Computational Fluid Dynamics, Vol. 10, pp. 13-25.

[13] Silverman, M., and Simon, M., 1974, “Flagellar Rotation and the Mechanism of bacterial Motility,” Nature, **249**, pp.73-74.

[14] Jiang, Y. and Przekwas, A. J., 1994, "Implicit, Pressure-Based Incompressible Navier-Stokes Equations Solver for Unstructured Meshes," AIAA-94-0305.

[15] Jiang, Y., Przekwas, A. J., and Wang, 1996, “Pressure-based high order accuracy flow solver on adaptive, mixed type unstructured grids,” AIAA-96-0417.

[16] Jiang, Y. and Chin-Yuan, P., 1997, “Computational Analysis of Oil Pumps with an Implicit Pressure Based Method Using Unstructured Mixed Element Grids,” SAE Technical Paper Series paper-970841, pp. 91-100.